

Density-Adaptive Kernel based Re-Ranking for Person Re-Identification

Ruopei Guo, Chun-Guang Li, *Member, IEEE*, Yonghua Li, Jiaru Lin, and Jun Guo

Abstract—Person Re-Identification (ReID) refers to the task of verifying the identity of a pedestrian observed from non-overlapping views of surveillance cameras networks. Recently, it has been validated that re-ranking could bring remarkable performance improvements for a person ReID system. However, the current re-ranking approaches either require feedbacks from users or suffer from burdensome computation cost. In this paper, we propose to exploit a density-adaptive smooth kernel technique to perform efficient and effective re-ranking. Specifically, we adopt a smooth kernel function to formulate the neighboring relationship amongst data samples with a density-adaptive parameter. Based on the new formulation, we present two simple yet effective re-ranking methods, termed *inverse* Density-Adaptive Kernel based Re-ranking (inv-DAKR) and *bidirectional* Density-Adaptive Kernel based Re-ranking (bi-DAKR), in which the local density information around each gallery sample is elegantly exploited. Moreover, we extend the proposed inv-DAKR and bi-DAKR to incorporate the available extra probe samples and demonstrate that the extra probe samples are able to improve the local neighborhood and thus further refine the ranking result. Extensive experiments are conducted on six benchmark datasets, including PRID450s, VIPeR, CUHK03, GRID, Market-1501 and Mars. Experimental results demonstrate that our proposals are effective and efficient.

I. INTRODUCTION

Person Re-Identification (ReID) refers to the task of verifying the identity of a pedestrian observed from non-overlapping views of surveillance cameras networks [1]. Due to its importance for the public security, it has received a lot of attention and increasingly becomes one of the most critical tasks in video analysis. However, the task of ReID is quite challenging, because the views captured by the surveillance cameras are under unconstrained conditions, and thus the obtained images contain large variations from the changes of pose, viewpoint, and illumination, occlusion, blur, background, etc.

To tackle these challenges, the standard pipeline of a person ReID system usually consists of two components: a) robust and discriminative feature extraction, and b) supervised metric learning. In the existing works, majority of efforts have been cast into extracting robust and discriminative visual representation. It has been verified that the local features, *i.e.*, color or oriented gradient histogram [2], [3], [4], [5], [6] are effective for person ReID, and combining multiple types of features, *i.e.*, color, texture, and spatial structure, is useful to find more informative matchings [7], [8], [9], [10], [11], [12], [13], [14], [15], [16]. On the other hand, supervised metric

learning methods—which learn a discriminative distance metric (or equivalently a low-dimensional subspace), in which the samples of same person are closer, could help the task of finding informative matchings [17], [18], [19], [20], [21], [22], [23]. In addition, simultaneous feature extraction and metric learning have also been investigated in the framework of deep convolutional neural network [24], [25], [26].

Recently, it has been reported that re-ranking could bring remarkable performance improvement for a person ReID system [27], [28], [29], [30], [31]. For example, feedback knowledge from users could be used to refine the ranking results, *i.e.*, [27], [28]. However, the feedback based refinement approaches build upon persistent users' feedbacks which are expensive burden on users. In [30], an approach called Supervised Smoothed Manifold (SSM) is proposed, in which an affinity graph is built to capture the manifold structure in the gallery set and the pairwise supervision information in the training set is propagated on the affinity graph. However, building the affinity graph is computationally expensive because all the samples in the gallery and training set are involved.

As an alternative way, the local neighborhood (e.g., the k nearest neighbors) of a given probe (*i.e.*, a query) and the neighborhoods of the k nearest neighbors of the probe are exploited to refine the ranking list. The typical approaches are mainly based on an interesting observation that reliable matchings between a probe and the samples in gallery set usually *share neighboring relationship mutually*. This leads to the re-ranking approaches based on so called k -reciprocal nearest neighbors [32], e.g., [29], [33], [34], [35], [36], [37]. In [33], [34], [36], the k -reciprocal nearest neighbors are directly considered as the top-ranked results. Recently, in [29], [35], the k -reciprocal nearest neighbors are encoded to refine the initial ranking list, or even integrated with local query expansion. In addition, in [37], extra visual features are combined with the k -reciprocal nearest neighbors to optimize the ranking list. While promising performance improvements have been shown on benchmark datasets, these methods still suffer from either the sensitivity to the tradeoff parameters or heavy computational burden.

Different from the prior works mentioned above, in this paper, we exploit a *density-adaptive kernel technique* to perform efficient and effective re-ranking for person ReID. To be more specific, we adopt a density-adaptive parameter to capture the local density information and then use it to formulate smooth kernel functions for finding the k nearest neighbors, the k inverse nearest neighbors, and the k reciprocal nearest neighbors. The used density-adaptive smooth kernel function quantifies the neighboring relationship of data samples via

R. Guo, C.-G. Li, Y. Li and J. Lin are with the School of Information and Communication Engineering, Beijing University of Posts and Telecommunications, Beijing 100876, P.R. China. E-mail: {guo2016; lichunguang; liyonghua; jrjin; guojun}@bupt.edu.cn.

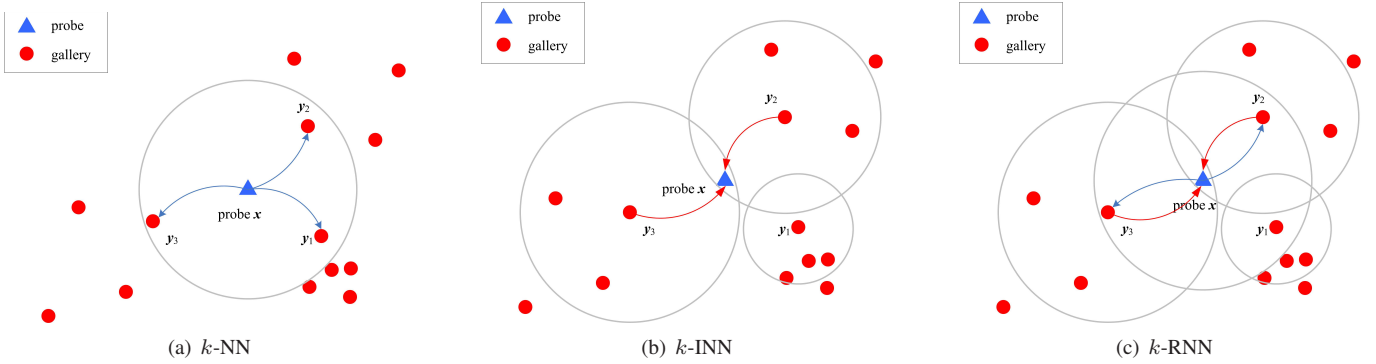


Fig. 1. Illustration for ranking and re-ranking in person ReID. (a) k -NN; (b) k -INN for inverse re-identification; (c) k -RNN, *i.e.*, k -NN integrated with k -INN, for bidirectional re-identification. The big circles indicate the boundary of the local neighborhood specified by k nearest neighbors with $k = 3$. In panel (a), the gallery samples \mathbf{y}_1 , \mathbf{y}_2 and \mathbf{y}_3 are the three nearest neighbors of the probe \mathbf{x} . If we consider k -NN in an inverse way, then only the gallery samples \mathbf{y}_2 and \mathbf{y}_3 are kept as shown in panel (b). When combining the results of k -NN and k -INN, we obtain the re-ranking result of k -RNN, which is shown in panel (c). In this case, the results of k -INN and k -RNN are the same.

a continuous (nonnegative) real number with *individually sample-specific scale*. Consequently, it is convenient to compute the inverse ranking list, and thus facilitates the task of forming the final re-ranking list by merging the inverse ranking list and the direct ranking list.

Specifically, we present two simple yet effective re-ranking methods, termed *inverse* Density-Adaptive Kernel based Re-ranking (inv-DAKR) and *bidirectional* Density-Adaptive Kernel based Re-ranking (bi-DAKR). Depending on how the probe samples are used, we divide the proposed re-ranking approaches into the following two groups:

- inv-DAKR and bi-DAKR: which are used in the setting when only a single probe sample and a set of gallery samples are available. The set of gallery samples are used to provide local density information and thus refine the ranking result to improve in the accuracy of a person ReID system. This setting is studied in our preliminary work [38].
- inv-DAKR+ and bi-DAKR+: which are used in the setting when a set of probe samples and a set of gallery samples are both available. The extra probe samples are able to improve the local neighborhood, provide more accurate local density information, and thus lead to remarkable improvements in the final re-ranking result.

This paper is a substantial extension of our preliminary work [38]. Compared to our previous work, the extensions include the following three aspects:

- We extend the proposed methods inv-DAKR and bi-DAKR into inv-DAKR+ and bi-DAKR+, respectively, in which the available extra probe samples are used to improve the re-ranking result.
- We extend the previous k -INN and k -RNN based re-ranking approaches into k -INN+ and k -RNN+, respectively, in which the extra probe samples are used to improve the local neighborhood in unsupervised way and thus lead to improvements in the re-ranking result.
- We conduct more extensive experimental evaluations on six benchmark datasets and show promising experimental results with thorough analysis and discussions.

Paper Outline. The remainder of this paper is organized as follows. Section II reviews the relevant work. Section III presents our proposals. Section IV shows experiments with discussions, and Section V concludes the paper.

II. RELATED WORK

To introduce our proposals, we review the prior methods for ranking or re-ranking by grouping them into three categories: a) k -nearest neighbors (k -NN) based methods, b) k -inverse nearest neighbors (k -INN) based methods, and c) k -reciprocal nearest neighbors (k -RNN) based methods. Denote the probe set as $\mathcal{X} = \{\mathbf{x}_1, \dots, \mathbf{x}_M\}$ and the gallery set as $\mathcal{Y} = \{\mathbf{y}_1, \dots, \mathbf{y}_N\}$, where \mathbf{x}_i and $\mathbf{y}_j \in \mathbb{R}^d$.

A. k -Nearest Neighbors based Methods

In k -NN based method, one calculates the distance between the probe $\mathbf{x}_i \in \mathcal{X}$ and each sample $\mathbf{y}_j \in \mathcal{Y}$, and then finds out a set of best matching candidates from the gallery set \mathcal{Y} . Precisely, finding the top- k best matching candidates can be formulated as follows:

$$\mathcal{N}(\mathbf{x}_i, k) = \arg \min_{\mathbf{y}_j \in \mathcal{Y}}^{[1:k]} \|\mathbf{y}_j - \mathbf{x}_i\|, \quad (1)$$

where $\|\cdot\|$ is a distance metric predefined or learnt from data, $\mathcal{N}(\mathbf{x}_i, k)$ is the set of the k -NN of the probe \mathbf{x}_i , and $[1 : k]$ indicates to take the first k candidates from the sorted list. The true matchings are expected to be included in $\mathcal{N}(\mathbf{x}_i, k)$. In Fig.1(a), the blue links starting from the probe \mathbf{x}_i to the gallery samples $\{\mathbf{y}_1, \mathbf{y}_2, \mathbf{y}_3\}$ illustrate result of k -NN with $k = 3$.

Finding reliable matchings for person ReID based on k -NN as in (1) is simple and efficient in implementation, however, the potentially useful information in the local neighborhood of gallery samples does not been exploited.

B. k -Inverse Nearest Neighbors based Methods

To exploit the potentially useful information in the local neighborhood of gallery samples for finding more reliable matchings, an intuitive and promising approach is to apply k -NN *inversely* on the gallery samples to search back for the

probe sample. This is called k -inverse nearest neighbors (k -INN) [32] based approach.

Specifically, for each gallery sample $\mathbf{y}_j \in \mathcal{Y}$, we find the best matchings of \mathbf{y}_j from $\{\mathbf{x}_i\} \cup \mathcal{Y}_{-j}$ where \mathcal{Y}_{-j} is the gallery set without the j -th sample \mathbf{y}_j . Denote the k -NN of \mathbf{y}_j as $\mathcal{N}(\mathbf{y}_j, k)$, which is defined as follows:

$$\mathcal{N}(\mathbf{y}_j, k) = \arg \min_{\mathbf{y} \in \{\mathbf{x}_i\} \cup \mathcal{Y}_{-j}}^{[1:k]} \|\mathbf{y} - \mathbf{y}_j\|. \quad (2)$$

If the probe \mathbf{x}_i is included in $\mathcal{N}(\mathbf{y}_j, k)$, then \mathbf{y}_j is viewed as one of the k -INN of \mathbf{x}_i .

To find out all the k -INN of \mathbf{x}_i , one has to compute $\mathcal{N}(\mathbf{y}_j, k)$ for all $j = 1, \dots, N$, where N is the size of the gallery set. Denote $\mathcal{I}(\mathbf{x}_i, k)$ as the set of all k -INN of \mathbf{x}_i . If $\mathbf{y}_j \in \mathcal{I}(\mathbf{x}_i, k)$, the probe \mathbf{x}_i is accepted as a good matching of \mathbf{y}_j ; otherwise, \mathbf{x}_i is rejected by \mathbf{y}_j as a bad matching. The true matching are expected to be included in $\mathcal{I}(\mathbf{x}_i, k)$.

In Fig. 1(b), the red links starting from the gallery samples $\{\mathbf{y}_2, \mathbf{y}_3\}$ to the probe \mathbf{x}_i illustrate the re-ranking by k -INN. In this case, although none of the sample in $\{\mathbf{y}_2, \mathbf{y}_3\}$ will identify \mathbf{x}_i as the best matching if only the (inverse) nearest neighbor (i.e., $k = 1$) is considered, \mathbf{y}_2 and \mathbf{y}_3 will find probe \mathbf{x}_i as their k nearest neighbor for $k = 3$.

When N is large, finding $\mathcal{I}(\mathbf{x}_i, k)$ is quite time consuming. Thus, in previous work, the k -INN of the probe sample is performed with only the k -NN of the probe sample in the gallery set due to the heavy computational burden. Unfortunately, performing k -INN on a small subset (i.e., the k -NN of the probe sample) of the gallery samples is incomplete and thus degenerates the recall rate of a person ReID system. Moreover, while the selected samples in $\mathcal{I}(\mathbf{x}_i, k)$ can further be sorted according to their distances to \mathbf{x}_i , the ambiguity of the potential candidate matchings and the local density information has not been properly captured. Besides, in previous work [33], [34], [35], [36], [29], k -INN has been considered as an intermediate step rather than as a re-ranking method and thus there is no valid evaluation on the performance of using k -INN for re-ranking.

C. k -Reciprocal Nearest Neighbors based Methods

Conceptually, “re-identification” (e.g., $a \leftrightarrow b$) consists of two single-directional implications (i.e., $a \rightarrow b$ and $a \leftarrow b$). In person ReID, the k -NN and k -INN based methods to find the best matchings can be viewed analogously as two single-directional implications. Thus it is natural to integrate k -NN and k -INN to form a re-identification with *bidirectional implications*. This is the core idea in the so-called k -RNN, which is illustrated in Fig. 1(c).

Denote the k -RNN of \mathbf{x}_i as $\mathcal{R}(\mathbf{x}_i, k)$. Then, $\mathcal{R}(\mathbf{x}_i, k)$ is the intersection of $\mathcal{N}(\mathbf{x}_i, k)$ and $\mathcal{I}(\mathbf{x}_i, k)$, i.e.,

$$\mathcal{R}(\mathbf{x}_i, k) = \mathcal{N}(\mathbf{x}_i, k) \cap \mathcal{I}(\mathbf{x}_i, k). \quad (3)$$

For a gallery sample \mathbf{y}_j , it does not belong to $\mathcal{R}(\mathbf{x}_i, k)$ as long as $\mathbf{y}_j \notin \mathcal{N}(\mathbf{x}_i, k)$ or $\mathbf{y}_j \notin \mathcal{I}(\mathbf{x}_i, k)$. Note that, judging a sample \mathbf{y}_j in or not in $\mathcal{N}(\mathbf{x}_i, k)$ or $\mathcal{I}(\mathbf{x}_i, k)$ is a binary decision with hard boundary. The ambiguity of the gallery sample \mathbf{y}_j

is ignored, especially for those gallery samples lying nearby the decision boundary.

The k -RNN is illustrated in Fig. 1(c). In this case, by integrating k -NN and k -INN, both \mathbf{y}_2 and \mathbf{y}_3 are the reliable candidate matchings to the probe sample \mathbf{x}_i when using $k = 3$.

In k -RNN, the dissimilarity between the probe sample \mathbf{x}_i and gallery sample $\mathbf{y}_j \in \mathcal{R}(\mathbf{x}_i, k)$ is usually measured by Jaccard distance, which is defined as follows:

$$\mathcal{J}(\mathbf{y}_j, \mathbf{x}_i) = 1 - \frac{|\mathcal{N}(\mathbf{y}_j, k) \cap \mathcal{N}(\mathbf{x}_i, k)|}{|\mathcal{N}(\mathbf{y}_j, k) \cup \mathcal{N}(\mathbf{x}_i, k)|}, \quad (4)$$

where $|\cdot|$ is to calculate the cardinality of a set. However, Jaccard distance as defined in (4) is built upon the overlapping of two local neighborhoods and thus is not accurate enough. In the previous work, e.g., [33], [34], [35], [36], [29], the ambiguity of the potential matching candidates in the returned k -INN is ignored and thus the previous k -RNN based methods are quite sensitive to parameter k .

To tackle the limitations aforementioned, we exploit a *density-adaptive kernel* technique to carry out the ideas in k -INN and k -RNN to perform efficient and effective re-ranking for person ReID. Specifically, rather than finding k -NN which has a hard boundary, in inv-DAKR and bi-DAKR, we put a smooth kernel function with a local density-adaptive parameter at each sample, and use the responses of the kernel function to define re-identification scorings which are continuous real value with sample-specific individual scale. Thus, inv-DAKR could be viewed as a smoothed version of the k -INN based re-ranking method and bi-DAKR could be viewed as a smoothed version of the k -RNN based re-ranking method. Unlike in k -INN and k -RNN methods, the ambiguity in the ranking lists and the local density information are properly accommodated and consequently the final performance will be improved.

III. OUR PROPOSALS: DENSITY-ADAPTIVE KERNEL BASED RE-RANKING

This section introduces a density-adaptive kernel function at first, and then describes our proposed density-adaptive kernel based re-ranking approaches, and finally present the analysis and discussions.

A. Density-Adaptive Kernel Function

To begin with, we introduce a density-adaptive kernel function, which lies in the core of our proposed re-ranking approaches.

Rather than just keeping a k -NN list, we adopt a smooth kernel function to compute the neighboringness of samples in order to accommodate the ambiguity in ranking list. Specifically, we define a smooth kernel function $\kappa(\mathbf{x}|\mathbf{x}_0, \sigma_0)$ where \mathbf{x}_0 is the location of the kernel and $\sigma_0 > 0$ is a local parameter. For convenience, we choose the *radial basis function*¹ to define $\kappa(\mathbf{x}|\mathbf{x}_0, \sigma_0)$, i.e.,

$$\kappa(\mathbf{x}|\mathbf{x}_0, \sigma_0) = \phi\left(\frac{\|\mathbf{x} - \mathbf{x}_0\|_2}{\sigma_0}\right), \quad (5)$$

¹The reason to use the radial basis function is owing to its explicit or implicit connection to distance function, which will be interpreted later.

where $\phi(\cdot) : \mathcal{R} \rightarrow \mathcal{R}^+$ is a monotonous basis function. By default, we use $\phi(t) = \exp(-t)$.

To make the kernel function $\kappa(\mathbf{x}|\mathbf{x}_0, \sigma_0)$ density-adaptive, the parameter σ_0 should be density-adaptive. In a denser region, the parameter σ_0 should be smaller in order to make the kernel function more selective (or sensitive) to reject more samples; whereas in a sparser region, the parameter σ_0 should be larger in order to make the kernel function relatively inclusive (or less sensitive) to accept more samples. In this sense, the expected parameter σ_0 should encode the density information in the local neighborhood of \mathbf{x}_0 . Thus, as suggested in [39], we define σ_0 as the distance of \mathbf{x}_0 to its k -th nearest neighbor $\mathbf{x}_0^{(k)}$, i.e.,

$$\sigma_0 = \|\mathbf{x}_0 - \mathbf{x}_0^{(k)}\|_2. \quad (6)$$

where $k \geq 1$ is a preset parameter. The σ_0 defined in (6) roughly encodes the density information in the local neighborhood of \mathbf{x}_0 .

The advantages of using a smooth kernel function with a density-adaptive parameter are at least twofold: a) the smoothness of the kernel function preserves the ambiguity of the potential candidates in the ranking list; and b) the local density-adaptive parameter endows the kernel function with an individually sample-specific scaling.

In the next subsections, we will show that the smooth kernel function with a density-adaptive local parameter is useful in formulating *smoothed* k -INN and *smoothed* k -RNN based re-ranking approaches.

B. Inverse Density-Adaptive Kernel based Re-Ranking (inv-DAKR)

Equipped with a density-adaptive kernel function, we are ready to present our inv-DAKR, which can be viewed as a smoothed k -INN based re-ranking approach. The key ingredient of inv-DAKR is that, instead of finding the list of k -INN directly, we use a smooth kernel function with a density-adaptive parameter to score all gallery samples.

Recall that the k -INN of the probe sample \mathbf{x}_i are defined by the list of gallery samples which inversely find the probe sample \mathbf{x}_i as one of their k -NN. As an analogue, we put a smooth kernel function $\kappa(\mathbf{x}|\mathbf{y}_j, \sigma_j)$ at each gallery sample \mathbf{y}_j with an adaptive local parameter σ_j where $j = 1, \dots, N$. Specifically, we use the *radial basis function* to define $\kappa(\mathbf{y}|\mathbf{y}_j, \sigma_j)$, i.e.,

$$\kappa(\mathbf{x}|\mathbf{y}_j, \sigma_j) = \phi\left(\frac{\|\mathbf{x} - \mathbf{y}_j\|_2}{\sigma_j}\right), \quad (7)$$

where σ_j is an adaptive local parameter which is defined as the distance of \mathbf{y}_j to its k -th nearest neighbor $\mathbf{y}_j^{(k)}$, i.e.,

$$\sigma_j = \|\mathbf{y}_j - \mathbf{y}_j^{(k)}\|_2. \quad (8)$$

In inv-DAKR, rather than finding the list of k -INN, we use the kernel function (7) which is located at each gallery sample \mathbf{y}_j to calculate a scoring *inversely* for the probe sample \mathbf{x}_i . Then, the re-ranking by inv-DAKR is conducted by sorting the N scorings for \mathbf{x}_i from the N gallery samples in descending order.

Compared to k -INN based re-ranking, owing to using a smoothed and density-adaptive kernel function, inv-DAKR has the following merits:

- 1) The ambiguity of the potential matching candidates is preserved by the adaptively scaled kernel function;
- 2) The proposed inv-DAKR computes N scorings $\{\kappa(\mathbf{x}_i|\mathbf{y}_j, \sigma_j)\}_{j=1}^N$ at first and then sort the N scorings only once, rather than sorting N samples individually N times in k -INN.² Thus, the computational cost in test stage is significantly reduced.

C. Bidirectional Density-Adaptive Kernel based Re-Ranking (bi-DAKR)

Recall that k -RNN is defined as the k reciprocal nearest neighbors, which are the intersection of the k -NN and the k -INN of the probe sample \mathbf{x}_i . That is, in k -RNN based re-ranking, we find out the lists of k -NN and k -INN at first and then take an intersection of two lists. Our bi-DAKR can be viewed as a smoothed k -RNN based re-ranking approach. In bi-DAKR, we compute the scorings via the density-adaptive kernel functions at first, then combine and sort the scorings to find the final list.

To implement a bidirectional re-identification, we gather the scorings from both the direct path and the inverse path. The deployed density-adaptive kernel functions are well-prepared to define the bidirectional re-identification. Note that:

- The kernel function located at the probe sample \mathbf{x}_i , i.e.,

$$\kappa(\mathbf{y}_j|\mathbf{x}_i, \sigma_i) = \phi\left(\frac{\|\mathbf{y}_j - \mathbf{x}_i\|_2}{\sigma_i}\right), \quad (9)$$

yields a scoring for the gallery sample \mathbf{y}_j , which can be viewed as *a belief from the probe sample \mathbf{x}_i looking for the gallery sample \mathbf{y}_j* , where $j = 1, \dots, N$.

- Similarly, the kernel function located at the gallery sample \mathbf{y}_j , i.e.,

$$\kappa(\mathbf{x}_i|\mathbf{y}_j, \sigma_j) = \phi\left(\frac{\|\mathbf{x}_i - \mathbf{y}_j\|_2}{\sigma_j}\right), \quad (10)$$

yields a scoring for the probe sample \mathbf{x}_i , which can be viewed as *a belief from the gallery sample \mathbf{y}_j looking for the probe sample \mathbf{x}_i* .

Have computed the $2N$ scorings from bidirectional paths, it is straightforward to combine them. While there are several ways to define the bidirectional scoring, as investigated in our preliminary work [38], we prefer to use the following form:

$$\chi(\mathbf{x}_i, \mathbf{y}_j) = \phi\left(\frac{\|\mathbf{y}_j - \mathbf{x}_i\|_2 \cdot \|\mathbf{x}_i - \mathbf{y}_j\|_2}{\sigma_i \sigma_j}\right). \quad (11)$$

Note that $\|\mathbf{y}_j - \mathbf{x}_i\|_2 \cdot \|\mathbf{x}_i - \mathbf{y}_j\|_2 = \|\mathbf{y}_j - \mathbf{x}_i\|_2^2$, we have that $\chi(\mathbf{x}_i, \mathbf{y}_j) = \phi\left(\frac{\|\mathbf{y}_j - \mathbf{x}_i\|_2^2}{\sigma_i \sigma_j}\right)$. The radical symmetry in functional form of $\phi\left(\frac{\|\cdot\|_2}{\sigma}\right)$ can reduce the calculation of the belief scorings $\{\chi(\mathbf{x}_i, \mathbf{y}_j)\}_{j=1}^N$. Another reason to choose the radial basis function is that the functional form of the radial basis function $\phi\left(\frac{\|\cdot\|_2}{\sigma}\right)$ has an explicit connection to the distance

²Note that the N density-adaptive parameters $\{\sigma_j\}_{j=1}^N$ could be computed in advance.

function, leading to a clear interpretation of DAKR, inv-DAKR and bi-DAKR as a smoothed k -NN, k -INN and k -RNN, respectively.

In practice, we compute in advance N parameters $\{\sigma_j\}_{j=1}^N$. Then, for a probe sample \mathbf{x}_i , we calculate N belief scorings $\{\chi(\mathbf{x}_i, \mathbf{y}_j)\}_{j=1}^N$, and produce the final result by sorting the N scores in descending order.

Compared to k -RNN, our bi-DAKR have the following advantages: a) the ambiguity in ranking list is preserved; b) the belief scorings are scaled individually and sample-specifically; and c) it is convenient to compute due to the symmetry in functional form.

D. Gain Further Re-ranking Performance with Extra Probe Samples

1) k -NN+, k -INN+ and k -RNN+: If a set of probe samples \mathcal{X} are available, we can use the probe samples, except for \mathbf{x}_i , to gain extra performance improvement. Specifically, we find the top- k best matching candidates to the probe \mathbf{x}_i with the augmented samples set $\mathcal{X}_{-i} \cup \mathcal{Y}$, i.e.,

$$\mathcal{N}(\mathbf{x}_i, k) = \arg \min_{\mathbf{y}_j \in \mathcal{X}_{-i} \cup \mathcal{Y}}^{[1:k]} \|\mathbf{y}_j - \mathbf{x}_i\|, \quad (12)$$

where \mathcal{X}_{-i} refers the probe samples except for the i -th sample \mathbf{x}_i . We term the k -NN based method with augmented samples as k -NN+. Note that the extra probe samples are viewed as ‘‘dummy samples’’, because they *occupy* the positions in the k -NN list but do not provide any supervision information (i.e., the identity).

Similarly, for k -INN, we can also find the best matchings of $\mathbf{y}_j \in \mathcal{Y}$ to the probe \mathbf{x}_i with the augmented samples $\mathcal{X} \cup \mathcal{Y}_{-j}$, i.e.,

$$\mathcal{N}(\mathbf{y}_j, k) = \arg \min_{\mathbf{y} \in \mathcal{X} \cup \mathcal{Y}_{-j}}^{[1:k]} \|\mathbf{y} - \mathbf{y}_j\|, \quad (13)$$

where \mathcal{Y}_{-j} refers to the gallery set except for \mathbf{y}_j . We term the k -INN based re-ranking method with augmented samples as k -INN+.

In k -INN+, while the extra probe samples are treated as ‘‘dummy samples’’ without any supervision information, they could properly improve the local neighborhood by occupying the positions in k -NN list and thus ‘‘push away’’ some wrong samples in the local neighborhood. When the incorrect samples are pushed away by some dummy samples, the re-ranking list will be refined, leading to improvements in the final performance.

As expected, by combining k -NN+ and k -INN+, we will have a k -RNN+ based re-ranking method. To demonstrate the effect of using the extra probe samples, we illustrate k -NN+, k -INN+, and k -RNN+ in Fig. 2. As could be observed, with one extra probe sample, the local neighborhood of \mathbf{y}_2 is improved, leading to different results of k -INN+ and k -RNN+.

2) *inv-DAKR+* and *bi-DAKR+*: In *inv-DAKR* and *bi-DAKR*, the local density-adaptive parameter σ_i is very important. If some extra probe samples \mathcal{X} are also available, we can define σ_i with the assistance of the extra probe samples. To be more specific, we set σ_i to the distance of \mathbf{x}_i to its k -th

nearest neighbor $\mathbf{x}_i^{(k)}$ with the samples in the augmented set $\mathcal{X} \cup \mathcal{Y}$ rather than with the samples only in \mathcal{Y} . We term the re-ranking methods of using *inv-DAKR* and *bi-DAKR* with the help of extra probe samples as *inv-DAKR+* and *bi-DAKR+*, respectively.

Remark. In k -INN+ and k -RNN+, the added extra probe samples improve the local neighborhood and thus bring performance improvements; whereas in *inv-DAKR+* and *bi-DAKR+*, the added extra probe samples not only improve the local neighborhood but also help to yield a more accurate density-adaptive parameter, leading to performance improvements. Nevertheless, the performance improvement might not be observed if the extra probe samples could not provide information to improve the local neighborhood of the gallery samples.

E. Analysis and Discussions

1) *Effectiveness of inv-DAKR and bi-DAKR*: Compared to the previous work [29], [33], [34], [36], [35], the effectiveness of *inv-DAKR* and *bi-DAKR* comes from three aspects. First, rather than *using a binary decision to judge in or not in the list of k-NN*, the used radial basis functions in *inv-DAKR* and *bi-DAKR* are able to model the ambiguity in the list of the potential candidates. Second, the used local parameter encodes the density information in each local neighborhood and thus makes the kernel functions in *inv-DAKR* and *bi-DAKR* are individually and sample-specifically scaled. Third, in *inv-DAKR* and *bi-DAKR*, all gallery samples are used to find the k -INN and k -RNN of the probe sample, rather than using only a small subset of the gallery samples (e.g., the k -NN of the probe sample). In particular, if the true matchings are not in the k -NN list of the probe sample, the true matchings have no chance to be found if k -INN and k -RNN are computed only with the k -NN of the probe sample.

2) *Efficiency of inv-DAKR and bi-DAKR*: The efficiency of *inv-DAKR* and *bi-DAKR* for re-ranking comes from the facts that the radical symmetry in kernel function formulation with the help of a density-adaptive parameter σ_j (which could be pre-computed in advance) reduced the redundant computation in sorting. Note that in *bi-DAKR*, only a density-adaptive parameter σ_i needs to be computed at the testing phase. For clarity, we list the detailed computation complexity of *inv-DAKR* and *bi-DAKR* compared to the baselines (k -NN, k -INN and k -RNN) in Table I. The comparison on times costs will also be provided in experiments.

IV. EXPERIMENTAL EVALUATIONS

To validate the efficiency and effectiveness of our proposals, we conduct experiments on six benchmark data sets, including GRID [40], PRID450S [41], VIPeR [10], CUHK03 [42], Market-1501 [43] and Mars [44].

A. Experimental Protocol

In our experiments, we use the standard protocol to split data. The matching accuracy at different ranks on data sets GRID, PRID450S, VIPeR, and CUHK03 is averaged over 10 trials. As baselines, we consider k -NN, k -INN, k -RNN, SSM

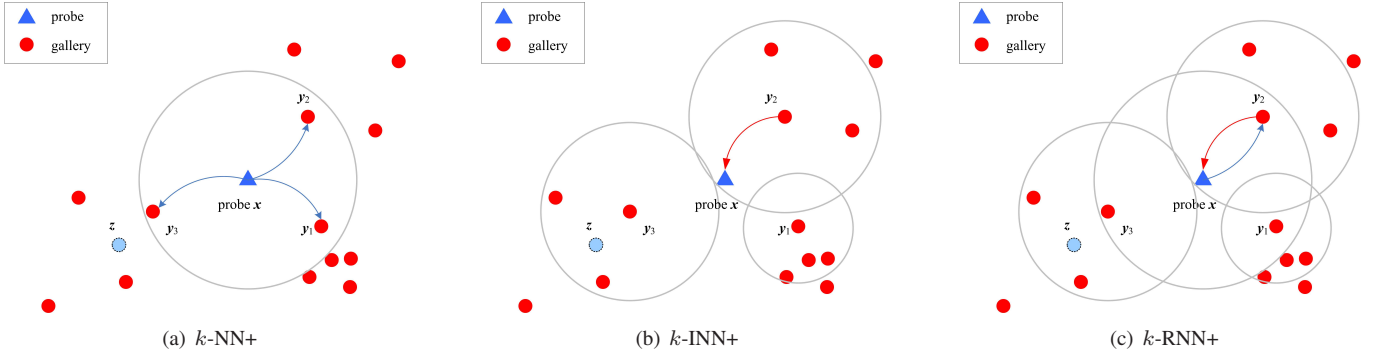


Fig. 2. Illustration for ranking and re-ranking when using an extra probe sample z . (a) k -NN+; (b) k -INN+ for inverse re-identification; (c) k -RNN+, *i.e.*, k -NN+ integrated with k -INN+ for bidirectional re-identification, where $k = 3$. The big circles indicate the boundary of the local neighborhood specified by three nearest neighbors. The blue faced small ball z indicates an extra probe sample. Compared to Fig. 1, while the result of k -NN in panel (a) does not change, the re-ranking results of k -INN in panel (b) are changed because the added “dummy” probe sample z changes the local neighborhood of the gallery sample y_3 such that y_3 no longer takes the probe sample x as one of its k nearest neighbors. Thus, when combining the results of k -NN and k -INN, the obtained re-ranking list of k -RNN is also changed as illustrated in panel (c).

TABLE I
COMPUTATION COMPLEXITY COMPARISON WITH UNILATERAL INFORMATION.

Methods	Complexity	
k -NN	$O(N + N \log_2 N)$	
k -INN	$O(N(N + 1)[1 + \log_2(N + 1)] + N \log_2 N)$	
k -INN+	$O(N(N + M)[1 + \log_2(N + M)] + N \log_2 N)$	
k -RNN	$O(N(N + 1)[1 + \log_2(N + 1)] + N(1 + \log_2 N))$	
k -RNN+	$O(N(N + M)[1 + \log_2(N + M)] + (N + M)(1 + \log_2(N + M)))$	
inv-DAKR bi-DAKR	off-line	$O(N^2 + N^2 \log_2 N)$
inv-DAKR+ bi-DAKR+		$O(N(N + M) + N(N + M) \log_2(N + M))$
inv-DAKR inv-DAKR+ bi-DAKR	on-line	$O(N + N \log_2 N)$
bi-DAKR		$O(2N + 2N \log_2 N)$
bi-DAKR+		$O((2N + M) + N \log_2 N + (N + M) \log_2(N + M))$

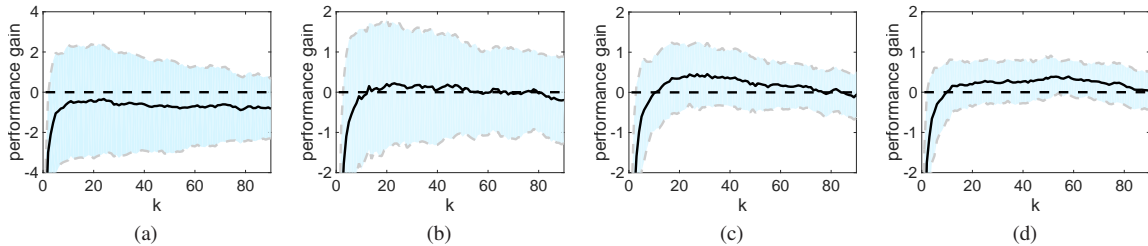


Fig. 3. Average performance gain of inv-DAKR as a function of k in perfect one-to-one matching scenario. (a): rank-1. (b): rank-5. (c): rank-10. (d): rank-20.

[30], and the re-ranking method in [29]. In addition, we use marker “+” to indicate the approaches which use the extra probe sample, including k -INN+, k -RNN+, inv-DAKR+ and bi-DAKR+.

Note that re-ranking can be viewed as a postprocessing step for person ReID. Our proposed re-ranking approaches inv-DAKR and bi-DAKR can be inserted into any person ReID pipeline. Therefore, we evaluate the proposed inv-DAKR and bi-DAKR on the six data sets with different combinations of feature extraction and metric learning.

For GRID, PRID450S, VIPeR, and CUHK03, we use LOMO [13] and GOG [12] features; whereas for Market-1501 and Mars, we use IDE features [43], [44]. For GRID, we also use ELF6 features [4]. Moreover, we conduct experiments on concatenating LOMO with GOG features and name it

as *Fusion*. In addition, another fusion feature is introduced for GRID by equally concatenating *Fusion* with unit ℓ_2 -norm ELF6 features and name it as *FusionAll*. On the other hand, for metric learning, we also consider Euclidean distance (ℓ_2 -norm), Mahalanobis distance, and KISSME [19] in both Market-1501 and Mars.

In inv-DAKR and bi-DAKR, the density-adaptive parameter σ_j depends on a preset parameter k , which changes from dataset to dataset. For each dataset, we report the results with an optimal k . In later subsections, we show the curves of average performance gain of using the proposed re-ranking methods with respect to varying parameter k , and also report an empirical rule to set a proper k .

To make the evaluation more systematic and clear, we divide the six benchmark datasets into three groups:

TABLE II
COMPARISON ON GRID, PRID450S, VIPeR, AND CUHK03 WITH DIFFERENT FEATURES.

Feature	Methods	PRID450S			VIPeR			CUHK03(labeled)			CUHK03(detected)			GRID		
		r=1	r=10	r=20	r=1	r=10	r=20	r=1	r=5	r=10	r=1	r=5	r=10	r=1	r=10	r=20
LOMO	k -NN	59.78	90.09	95.29	41.08	82.34	91.27	50.85	81.38	91.14	44.45	78.70	87.65	16.56	41.84	52.40
	k -INN	51.38	90.04	94.58	35.32	82.25	90.85	40.14	80.73	90.74	36.65	78.15	88.75	21.52	44.88	55.68
	k -RNN	45.51	84.80	91.69	29.40	77.47	90.28	40.74	78.03	89.09	36.70	73.35	84.65	19.44	42.96	54.56
	inv-DAKR	59.24	90.44	95.29	41.61	83.10	91.84	52.56	83.08	91.74	47.35	79.90	89.75	19.84	45.44	56.24
	bi-DAKR	61.42	92.40	96.93	42.97	83.86	92.41	53.45	84.74	92.84	48.10	80.80	90.05	19.60	44.48	56.40
	k -INN+	58.09	90.53	94.80	41.36	83.64	91.71	52.05	83.63	91.79	46.75	81.05	89.30	21.60	45.12	56.00
	k -RNN+	60.31	90.04	94.76	41.11	82.56	91.36	51.00	81.58	91.09	44.55	78.70	87.40	17.36	42.88	54.48
	inv-DAKR+	60.67	91.47	96.00	43.07	83.83	92.12	53.00	82.48	89.19	48.90	77.95	87.50	19.68	44.56	55.68
	bi-DAKR+	63.29	93.02	97.29	43.83	84.27	92.66	55.11	85.58	92.99	50.00	82.30	90.70	19.36	44.48	56.24
GOG	k -NN	68.00	94.36	97.64	49.68	88.67	94.53	68.47	90.69	95.84	64.10	88.40	94.30	24.80	58.40	68.88
	k -INN	53.11	94.22	97.60	41.61	87.41	94.59	52.50	90.49	96.95	49.10	87.55	94.35	27.44	57.84	68.56
	k -RNN	47.38	90.22	96.09	34.18	83.16	92.88	56.26	87.28	94.54	52.20	85.80	92.30	24.40	56.40	67.20
	inv-DAKR	65.02	94.98	98.00	48.73	89.18	94.97	70.32	92.54	97.20	67.20	90.30	95.60	26.00	58.00	68.72
	bi-DAKR	68.98	95.82	98.62	50.66	90.19	95.51	71.87	93.24	97.70	68.80	90.50	95.80	27.12	60.16	70.96
	k -INN+	64.71	95.42	97.96	50.22	89.34	95.00	70.87	93.14	97.45	67.05	90.65	95.60	28.08	58.64	69.04
	k -RNN+	68.67	94.53	97.60	49.75	88.32	93.89	68.82	90.99	95.94	64.95	88.35	94.30	25.12	58.80	69.68
	inv-DAKR+	68.13	95.87	98.53	51.14	89.78	95.22	73.23	92.54	96.45	68.55	90.95	95.40	26.32	57.52	67.60
	bi-DAKR+	71.73	96.36	98.89	52.44	90.44	95.82	74.98	94.44	97.90	70.20	92.15	96.55	26.96	59.76	70.32
Fusion	k -NN	72.04	95.96	98.53	53.26	90.95	95.73	71.87	92.64	96.80	68.05	90.15	94.95	27.04	59.36	70.00
	k -INN	55.38	95.33	97.96	43.80	89.78	95.25	53.55	91.99	97.50	50.30	89.65	95.60	28.00	58.96	68.56
	k -RNN	49.07	91.38	96.44	37.44	85.73	93.73	59.81	90.34	95.64	56.10	87.25	93.35	25.60	57.12	67.60
	inv-DAKR	68.58	96.00	98.44	52.53	90.57	95.89	73.53	94.24	98.15	70.65	92.10	96.25	28.16	59.60	69.84
	bi-DAKR	73.16	97.02	99.11	54.34	91.58	96.33	75.08	95.14	98.35	72.85	92.05	96.45	28.00	61.52	71.36
	k -INN+	70.27	96.22	98.53	52.94	91.27	95.73	73.62	94.35	97.95	72.40	92.30	96.40	28.64	59.44	69.36
	k -RNN+	73.20	95.82	98.49	53.32	90.70	95.41	72.47	92.84	96.70	68.85	90.15	94.90	27.04	60.48	70.56
	inv-DAKR+	71.51	96.76	98.93	53.70	91.36	96.01	76.73	94.44	97.30	72.35	92.60	96.35	27.12	59.36	68.96
	bi-DAKR+	75.29	97.38	99.07	55.89	91.93	96.87	78.48	95.79	98.40	75.30	93.40	97.00	27.60	61.44	70.72
	Zhong's [29]	72.36	96.27	98.71	53.70	91.65	96.65	73.42	93.74	97.29	69.60	91.50	95.55	28.00	60.40	70.64
	SSM[30]	72.98	96.76	99.11	53.73	91.49	96.08	76.63	94.59	97.95	72.70	92.40	96.05	27.20	61.12	70.56

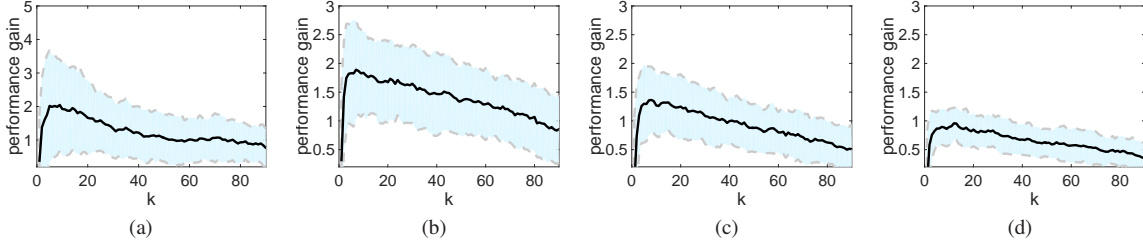


Fig. 4. Average performance gain of bi-DAKR as a function of k in perfect one-to-one matching scenario. (a): rank-1. (b): rank-5. (c): rank-10. (d): rank-20.

- Datasets with perfect single-shot matching, which include PRID450s, VIPeR, and CUHK03.
- Dataset with imperfect single-shot matching, which includes GRID.
- Datasets with multiple-shot matching, which include Market-1501 and Mars.

B. Experiments on Datasets with Perfect Single-Shot Matching: PRID450s, VIPeR, and CUHK03

1) *Datasets Descriptions*: Both PRID450s and VIPeR datasets capture walking person images from two disjoint cameras and mainly suffer from varying viewpoints, illuminations and poses. PRID450s includes totally 450 images of 225 pedestrians, and VIPeR includes 316 pairs of images of 316 pedestrians. In experiments, both datasets have half of the image pairs for training and half of the image pairs for testing.

Different from PRID450s and VIPeR, CUHK03 collects 13,164 images of 1,360 walking people from six disjoint cameras. CUHK03 suffers from misalignments, occlusions and body part missing and thus it is closer to real surveillance

scenario. Except for the manually cropped pedestrian images, it also includes pedestrian images detected from state-of-art pedestrian detector. In experiments, 200 images of 100 persons are used for testing and around 13,000 images of 1260 people are used for training.

We refer these three datasets as *perfect single-shot matching* because in testing phase, the samples in gallery set are one-to-one correspondence to the samples in probe set.

2) *Experimental Results*: We show experimental results in Table II. As could be read, the proposed inv-DAKR and bi-DAKR show notable improvements compared to the baseline results of k -NN.

If the set of probe samples are available, we can use them to further improve the re-ranking results. As can be found that both inv-DAKR+ and bi-DAKR+ yield further improvements over inv-DAKR and bi-DAKR. Compared to inv-DAKR, the improvements of bi-DAKR+ are more notable. On average, inv-DAKR+ improved over inv-DAKR around 3% and bi-DAKR+ improved over bi-DAKR around 5%.

Note that, the set of probe samples are also used in the state-

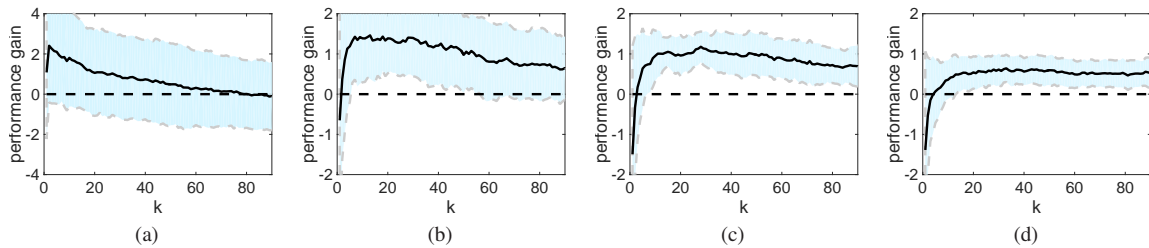


Fig. 5. Average performance gain of inv-DAKR+ as a function of k in perfect one-to-one matching scenario. (a): rank-1. (b): rank-5. (c): rank-10. (d): rank-20.

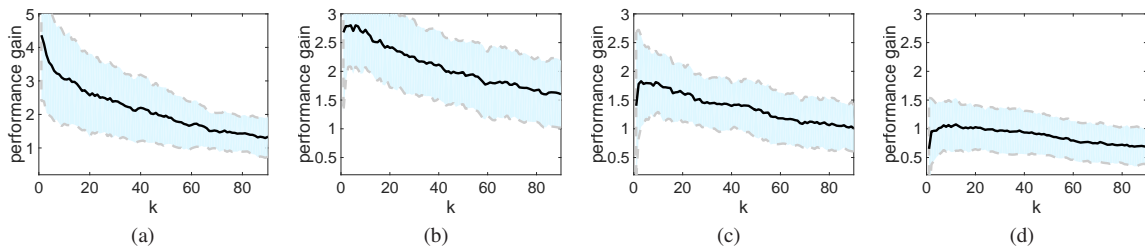


Fig. 6. Average performance gain of bi-DAKR+ as a function of k in perfect one-to-one matching scenario. (a): rank-1. (b): rank-5. (c): rank-10. (d): rank-20.

of-arts re-ranking approach in [29] to find reciprocal samples. While more sophisticated approaches are involved in [29] and [30], our simple proposals still yield superior or comparable results. In later subsection, we will show that our proposed approaches are much cheaper in computational cost.

3) *Analysis and Discussions*: To give a comprehensive understanding of the experimental results, we calculate the average performance gain with respect to the k -NN baseline as a function of the parameter k in Fig. 3, 4, 5, and 6.

On these three datasets, the performance of bi-DAKR is more promising than inv-DAKR. This suggests that integrating the re-identification information in both the direct way and the inverse way is quite useful. On contrary, we observe that both k -INN and k -RNN yield inferior results, which are even worse than the k -NN baselines. These results confirm that using a smooth kernel function with a local density-adaptive parameter to accommodate the ambiguity into the re-ranking list is effective.

If the probe samples are used, as could be observed from Fig. 5 and 6 that not only the average performance gains of inv-DAKR+ and bi-DAKR+ increase on average but also the variances are reduced. Especially, when using a smaller k , as illustrated at the beginning of the curves, the performance improvements are significant. In addition, we also observed that both k -INN+ and k -RNN+ perform better than k -NN. These results suggest that in the *perfect single-shot matching scenario*, putting the probe samples into gallery set does help to improve the re-ranking results.

In addition, in Table II, from LOMO features to Fusion features through all the three datasets, we can observe performance gain of using the probe set. The reason is that the more discriminative and robust the features are, the better feature space it will build for local contexture detecting method to work. Since GOG features are more robust than LOMO features and weaker than Fusion features which are obtained by combining with LOMO features, the performance gain

comes from the robustness of the feature. Compared to VIPeR and PRID450s, it is more obvious that k -INN+ and k -RNN+ improve more notable in CUHK03.

C. Experiments on Dataset with Imperfect Single-Shot Matching: GRID

1) *Datasets Descriptions*: GRID is basic data set for person re-identification task and contains 250 pedestrian image pairs. As usual, 125 image pairs are used for training and 125 image pairs are used for testing. Besides, there are also 775 images in the gallery set but the 775 images do not match to any person in the probe. Therefore, we call it *imperfect single-shot matching* because the gallery set do not have an one-to-one matching to the probe.

2) *Experimental Results and Discussions*: We list the experimental results in the last few columns of Table II and in Table III. While our proposed inv-DAKR and bi-DAKR still show notable performance improvements compared to k -NN, there are two differences: a) The performance of inv-DAKR can compete to or even outperform bi-DAKR; b) The performance difference between using the probe set and not using the probe set is minor. Note that except for 125 pairs of probe samples, the gallery set also includes 775 irrelevant images, which are not matching to any probe samples. When the 775 irrelevant images are added, they cannot provide useful information to improve the local neighborhood of the gallery samples. Thus, the performance improvements in k -INN+, k -RNN+, inv-DAKR+, and bi-DAKR+ over their counterpart methods are relatively minor.

To have more understanding of the experimental results, we calculate the curves of average performance gain with respect to the corresponding result of k -NN and show them as functions of parameter k in Fig. 7, 9, 8 and 10, respectively. As could be perceived that, the performance gain of using and not using the probe set is minor. This is because that, while the 125 pairs of probe samples could provide some useful

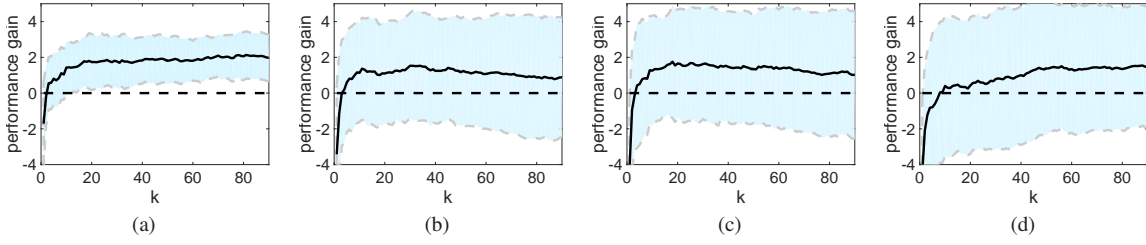


Fig. 7. Average performance gain of of inv-DAKR as a function of k in imperfect one-to-one matching scenario. (a): rank-1. (b): rank-5. (c): rank-10. (d): rank-20.

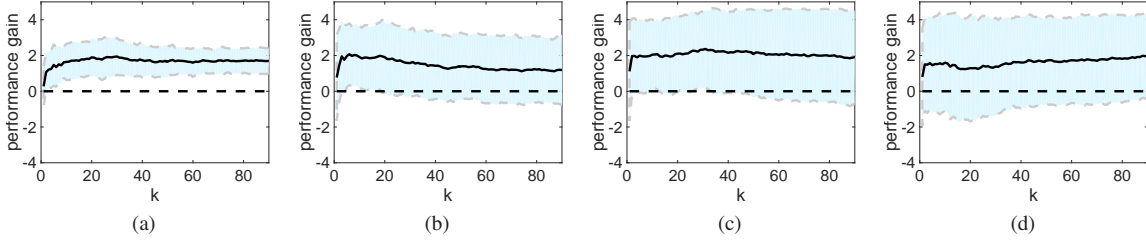


Fig. 8. Average performance gain of of bi-DAKR as a function of k in imperfect one-to-one matching scenario. (a): rank-1. (b): rank-5. (c): rank-10. (d): rank-20.

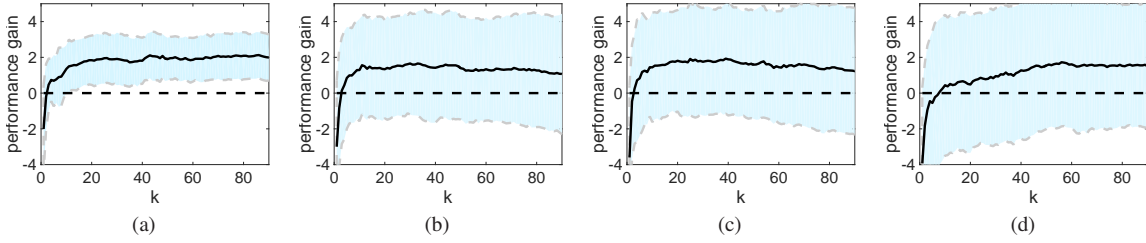


Fig. 9. Average performance gain of inv-DAKR+ as a function of k in imperfect one-to-one matching scenario. (a): rank-1. (b): rank-5. (c): rank-10. (d): rank-20.

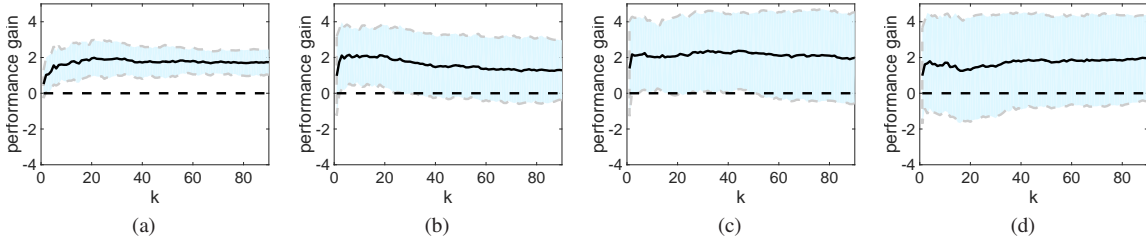


Fig. 10. Average performance gain of bi-DAKR+ as a function of k in imperfect one-to-one matching scenario. (a): rank-1. (b): rank-5. (c): rank-10. (d): rank-20.

information, they only take a small proportion (i.e., around 25%). The added 775 irrelevant images will dilute the true distribution and thus eliminate the performance improvements.

D. Experiments on Datasets with Multiple-Shot Matching: Market-1501 and Mars

1) *Datasets Descriptions*: Market-1501 is a large data set for person Re-Id task generated in an open environment. There are 32,668 boxes of 1,501 walking people captured from six surveillance cameras net in campus, where 2,793 distracters are included. In the experiment, 19,732 images of 750 identities are used for training and 12,936 images of 751 identities are used for testing. Besides, 3,368 images are randomly selected from total 12,936 images as probe and there

are on average around 17.5 ground truths for each probe. Mars is a video extension of the Market-1501 and contains around 20,000 images for 1,261 identities. There are 8,298 images of 631 identities are used for training and the rest are used for testing. Similarly, 1,980 images of 630 identities are selected as probe set from total 12,180 images where 3,248 distracters are included and there are on average around 12.8 ground truths for each probe.

Since there are multiple ground truths for both of them, we refer these two datasets *multiple-shot matching* scenario. Note that, in Market-1501 and Mars, the probe is randomly picked out from the total gallery set. That is, the probe set is included in the gallery set. Thus, we do not consider the setting of adding the probe samples to the gallery set.

TABLE III

COMPARISON ON GRID WITH DIFFERENT FEATURES.

Feature	Metric	Methods	r=1	r=10	r=20
ELF6	Euc	<i>k</i> -NN	4.88	20.32	26.24
		<i>k</i> -INN	7.20	21.28	31.60
		<i>k</i> -RNN	6.72	19.68	26.20
		inv-DAKR	8.32	22.80	31.20
		bi-DAKR	6.32	22.32	28.80
		<i>k</i> -INN+	6.96	22.56	31.28
		<i>k</i> -RNN+	5.28	21.36	30.24
		inv-DAKR+	8.80	22.64	30.4
ELF6	XQDA	bi-DAKR+	6.88	22.80	28.88
		<i>k</i> -NN	8.64	30.48	44.32
		<i>k</i> -INN	13.60	38.96	50.88
		<i>k</i> -RNN	10.96	37.44	48.72
		inv-DAKR	13.36	40.16	52.08
		bi-DAKR	11.28	39.52	52.40
		<i>k</i> -INN+	13.52	39.12	50.48
		<i>k</i> -RNN+	9.92	34.16	46.96
LOMO	Euc	inv-DAKR+	13.28	40.48	52.16
		bi-DAKR+	11.36	39.44	52.24
		<i>k</i> -NN	15.20	30.80	36.40
		<i>k</i> -INN	14.64	35.44	42.64
		<i>k</i> -RNN	13.36	30.80	38.16
		inv-DAKR	16.00	35.44	43.76
		bi-DAKR	17.84	34.16	41.44
		<i>k</i> -INN+	14.64	35.76	43.76
GOG	Euc	<i>k</i> -RNN+	16.56	32.16	38.56
		inv-DAKR+	14.80	35.68	44.08
		bi-DAKR+	17.04	34.24	41.28
		<i>k</i> -NN	13.28	33.76	44.40
		<i>k</i> -INN	15.44	34.88	42.40
		<i>k</i> -RNN	12.80	30.72	39.36
		inv-DAKR	16.56	34.96	43.20
		bi-DAKR	16.00	36.40	44.96
Fusion	Euc	<i>k</i> -INN+	15.60	35.28	42.96
		<i>k</i> -RNN+	14.72	34.40	44.08
		inv-DAKR+	14.88	34.96	41.28
		bi-DAKR+	15.44	36.32	44.72
		<i>k</i> -NN	14.72	35.44	45.84
		<i>k</i> -INN	16.00	35.76	43.92
		<i>k</i> -RNN	14.64	32.56	41.02
		inv-DAKR	18.16	37.04	46.00
FusionAll	Euc	bi-DAKR	18.64	37.68	46.00
		<i>k</i> -INN+	16.88	35.52	45.36
		<i>k</i> -RNN+	15.92	36.48	45.60
		inv-DAKR+	17.44	37.44	43.44
		bi-DAKR+	18.56	37.92	45.52
		<i>k</i> -NN	14.80	35.60	46.24
		<i>k</i> -INN	15.04	35.76	43.44
		<i>k</i> -RNN	13.76	31.92	39.68
FusionAll	XQDA	inv-DAKR	17.68	36.08	45.12
		bi-DAKR	17.76	37.20	46.08
		<i>k</i> -INN+	16.40	36.32	44.32
		<i>k</i> -RNN+	16.24	36.64	45.12
		inv-DAKR+	18.40	37.28	45.60
		bi-DAKR+	17.68	37.68	45.76
		<i>k</i> -NN	27.20	61.12	71.20
		<i>k</i> -INN	28.56	59.92	70.00
		<i>k</i> -RNN	26.08	57.84	69.20
		inv-DAKR	28.88	60.40	70.88
FusionAll	XQDA	bi-DAKR	28.08	62.40	72.08
		<i>k</i> -INN+	29.52	60.64	70.48
		<i>k</i> -RNN+	27.44	61.84	71.84
		inv-DAKR+	28.80	60.96	70.88
		bi-DAKR+	28.24	62.56	72.24
		Zhong's[29]	28.24	61.60	71.92
SSM[30]	27.60	62.56	71.60		

TABLE IV
COMPARISON ON MARKET-1501 WITH LOMO FEATURES IN DIFFERENT METRICS.

Metric	Methods	r=1	r=5	r=10	mAP
Euc	<i>k</i> -NN	15.11	27.23	33.70	4.03
	<i>k</i> -INN	10.68	25.92	32.81	2.05
	<i>k</i> -RNN	15.17	27.55	33.73	3.09
	inv-DAKR	15.65	27.35	33.67	4.18
	bi-DAKR	15.77	27.67	34.35	4.24
XQDA	Zhong's[29]	15.83	27.02	33.17	4.55
	<i>k</i> -NN	28.56	51.60	61.82	13.70
	<i>k</i> -INN	23.81	50.50	61.43	8.46
	<i>k</i> -RNN	28.92	52.02	62.29	7.78
	inv-DAKR	30.97	52.49	62.68	15.10
KISSME	bi-DAKR	30.52	52.97	63.21	14.86
	Zhong's[29]	31.12	51.48	61.37	15.86
	<i>k</i> -NN	41.60	63.87	73.43	19.37
	<i>k</i> -INN	31.80	61.22	69.36	14.59
	<i>k</i> -RNN	41.81	62.89	70.49	14.90
Mahal	inv-DAKR	43.41	63.51	72.33	21.97
	bi-DAKR	43.76	65.56	75.24	21.92
	Zhong's[29]	45.16	64.01	73.16	23.45
	<i>k</i> -NN	35.04	55.73	65.62	13.78
	<i>k</i> -INN	26.99	52.08	60.99	11.47
Mahal	<i>k</i> -RNN	35.51	54.25	61.13	10.26
	inv-DAKR	36.79	55.46	63.81	16.93
	bi-DAKR	37.77	58.19	67.58	16.83
	Zhong's[29]	37.86	56.00	65.50	16.23

TABLE V

COMPARISON ON MARKET-1501 WITH RESNET-50-IDE FEATURES IN DIFFERENT METRICS.

Metric	Methods	r=1	r=5	r=10	mAP
Euc	<i>k</i> -NN	69.51	83.94	88.69	44.45
	<i>k</i> -INN	56.95	82.96	88.66	32.90
	<i>k</i> -RNN	69.54	84.32	88.75	36.59
	inv-DAKR	69.48	84.41	88.66	45.27
	bi-DAKR	69.66	84.62	89.52	45.50
	Zhong's[29]	71.32	83.43	88.42	49.01
XQDA	<i>k</i> -NN	75.53	88.63	91.66	53.03
	<i>k</i> -INN	64.55	88.66	92.52	32.90
	<i>k</i> -RNN	75.74	88.69	91.75	39.00
	inv-DAKR	76.87	89.43	92.67	54.58
	bi-DAKR	76.90	89.58	93.17	54.88
KISSME	Zhong's[29]	77.58	88.57	91.51	57.94
	<i>k</i> -NN	77.52	89.61	93.05	53.88
	<i>k</i> -INN	66.09	89.58	93.29	41.92
	<i>k</i> -RNN	77.64	89.79	93.11	43.14
	inv-DAKR	78.95	90.26	93.53	55.95
Mahal	bi-DAKR	78.92	90.68	94.24	55.88
	Zhong's[29]	79.90	89.52	93.14	59.37
	<i>k</i> -NN	77.20	89.82	92.99	52.99
	<i>k</i> -INN	65.41	89.34	93.11	42.03
	<i>k</i> -RNN	77.35	89.93	92.93	46.73
Mahal	inv-DAKR	78.74	90.08	93.71	54.84
	bi-DAKR	78.41	90.80	94.00	55.09
	Zhong's[29]	79.13	89.82	93.29	57.73

2) *Experimental Results and Discussions:* We show experimental results on Market-1501 and Mars in Table V and VII. Again, we can observe the performance improvements over the results of the baseline method *k*-NN. Different from *k*-INN, *k*-RNN, our proposed inv-DAKR and bi-DAKR still brings performance improvements. Compared to the re-ranking method proposed in [29], while the accuracy of inv-DAKR and bi-DAKR is inferior on rank-1 and mAP, the results on rank-5, rank-10 and rank-20 are competitive to or even superior.

It should be noted that, both local query expansion and sophisticated weighting strategies involving Jaccard distance are

TABLE VI
COMPARISON ON MARKET-1501 WITH CAFFE FEATURES IN DIFFERENT METRICS.

Metric	Methods	r=1	r=5	r=10	mAP
Euc	k -NN	55.91	76.84	83.79	31.66
	k -INN	45.19	75.03	83.05	19.84
	k -RNN	56.15	77.02	83.85	23.80
	inv-DAKR	56.95	77.26	83.91	32.41
	bi-DAKR	56.95	77.41	84.53	32.58
	Zhong's[29]	58.17	76.90	83.52	35.22
XQDA	k -NN	61.73	81.03	87.29	37.62
	k -INN	50.86	80.97	87.65	31.20
	k -RNN	62.05	81.50	87.23	26.53
	inv-DAKR	63.63	82.19	88.30	39.56
	bi-DAKR	63.72	82.27	88.42	39.26
	Zhong's[29]	64.70	81.18	87.23	41.63
KISSME	k -NN	61.05	81.00	86.46	36.75
	k -INN	49.67	80.40	86.94	29.02
	k -RNN	61.31	81.44	86.97	23.52
	inv-DAKR	63.45	81.80	87.74	38.91
	bi-DAKR	62.86	82.10	87.47	38.51
	Zhong's[29]	63.27	80.88	86.43	40.50
Mahal	k -NN	60.45	79.96	86.16	35.52
	k -INN	49.79	80.11	86.52	24.31
	k -RNN	60.57	80.29	86.37	27.39
	inv-DAKR	62.20	80.97	87.11	36.93
	bi-DAKR	61.64	81.15	87.26	36.80
	Zhong's[29]	62.26	80.29	86.28	38.57

TABLE VII
COMPARISON ON MARS WITH IDE FEATURES AND IN DIFFERENT METRICS.

Metric	Methods	r=1	r=5	r=20	mAP
Euc	k -NN	60.81	77.93	87.88	41.24
	k -INN	49.34	76.52	86.21	34.34
	k -RNN	61.16	77.73	85.91	34.57
	inv-DAKR	61.77	78.08	87.83	42.72
	bi-DAKR	61.67	79.39	88.54	42.77
	Zhong's[29]	62.53	78.23	87.58	44.09
XQDA	k -NN	65.51	81.72	90.10	46.85
	k -INN	52.93	80.81	89.70	39.20
	k -RNN	65.76	82.02	89.04	42.63
	inv-DAKR	66.46	82.63	90.91	48.58
	bi-DAKR	66.46	82.93	91.21	48.76
	Zhong's[29]	67.07	81.82	90.10	50.61
KISSME	k -NN	64.95	81.01	89.90	44.20
	k -INN	52.68	79.55	87.73	38.81
	k -RNN	65.15	81.01	87.17	40.48
	inv-DAKR	64.90	82.37	90.05	47.12
	bi-DAKR	66.16	82.68	91.57	47.55
	Zhong's[29]	66.46	81.16	90.10	48.22
Mahal	k -NN	63.33	80.51	87.74	42.12
	k -INN	51.97	77.58	86.11	37.76
	k -RNN	63.59	79.80	85.40	38.22
	inv-DAKR	63.99	80.56	89.19	45.84
	bi-DAKR	65.40	81.62	90.86	46.49
	Zhong's[29]	65.40	80.71	89.29	45.94

used to refine the ranking list in [29]; whereas our approaches are completely built on a smooth kernel function with local density-adaptive parameter. When the size of the neighborhood grows, it is hard for the local query expansion and Jaccard distance to find good matchings. Moreover, the re-ranking method proposed in [29] is sensitive to used parameters, e.g., k_1 , k_2 , λ ; whereas our inv-DAKR and bi-DAKR are not that sensitive to the parameter k , which will be shown in subsection IV-E.

To gain more understanding of the experimental results, we again show the average performance gain of inv-DAKR and

bi-DAKR with respect to the result of k -NN as functions of the parameter k , in Fig. 11 and 12. From these curves, we observe that, compared to inv-DAKR, bi-DAKR is more promising.

E. Performance Evaluation on Parameter k and Discussions

In the proposed inv-DAKR and bi-DAKR, the smooth kernel function adopts a local-density adaptive parameter σ_j , which is set as the distance of \mathbf{x}_j to its k -th nearest neighbor $\mathbf{x}_j^{(k)}$. Thus, it is interesting to evaluate the sensitivity of the performance of inv-DAKR and bi-DAKR to parameter k . To this end, we compute the average performance gains of inv-DAKR and bi-DAKR over the baseline algorithm (k -NN) for accuracy at rank-1, rank-5 rank-10 and rank-20 in three different scenario: a) *Perfect single-shot matching*, b) *Imperfect single-shot matching* and c) *Multiple-shot matching*, and show each of the results as a function of parameter k in Figs. 3 to 11.

Through all the results in Figs. 3 to 11, we observe that: while the proposed inv-DAKR and bi-DAKR both yield promising improvements, bi-DAKR yields consistent improvements on all datasets.

When the extra probe samples are available, using both the probe samples and the gallery samples could provide more accurate local density parameter to reveal the true local distribution of the samples. Thus, inv-DAKR+ and bi-DAKR+ improve the performance over inv-DAKR and bi-DAKR, respectively. The experiments on datasets with perfect single-shot matching, as shown in Section IV-B confirm this point. In such scenario, we suggest to set parameter k to the number of 5% of the testing set.

On datasets with multiple-shot matching, from the curves in Fig. 11 and 12, we found that the proper value of parameter k is relevant to the average number of ground-truth matchings in datasets. For example, there are on average 17.8 ground-truth matchings in Market-1501 and thus the performance of bi-DAKR gets to be stable when $k \geq 18$. Compared to bi-DAKR, which uses the re-identification from two directions, inv-DAKR needs a larger value of k to get relatively stable performance. Therefore, we suggest to set k to the average number of the groundtruth matchings in datasets for multiple-shot matching scenario.

F. Comparison on Time Costs

For fair comparison, we list the computational time costs of all methods in Table VIII. For dataset CHUK03, we report time costs of the labeled dataset. The sizes listed in Table VIII are the number of test data.

It shows that the time costs of our proposals are much cheaper than the re-ranking method in [29], especially when the data set is large. The method in [29] needs to find k -reciprocal nearest neighbors, expand local query sequence, and compute Jaccard distance; whereas in our inv-DAKR and bi-DAKR, only a density-adaptive kernel function is needed to be evaluated. Though slightly defeated by the re-ranking method in [29] at rank-1 and mAP, our inv-DAKR and bi-DAKR are much simple, faster, and having improved results at rank-5, rank-10 and rank-20.

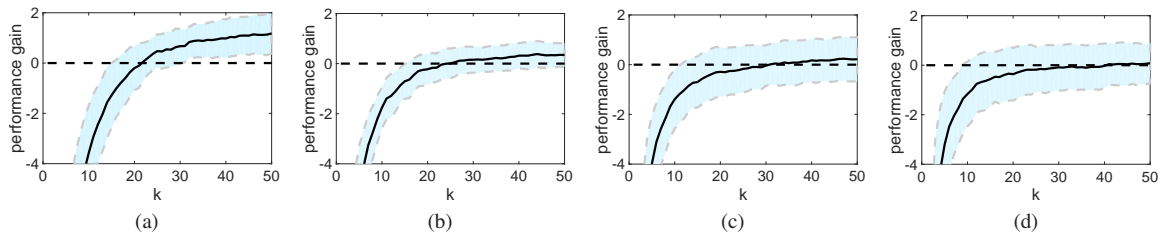


Fig. 11. Average performance gain of inv-DAKR as a function of k in multiple-to-multiple matching scenario. (a): rank-1. (b): rank-5. (c): rank-10. (d): rank-20.

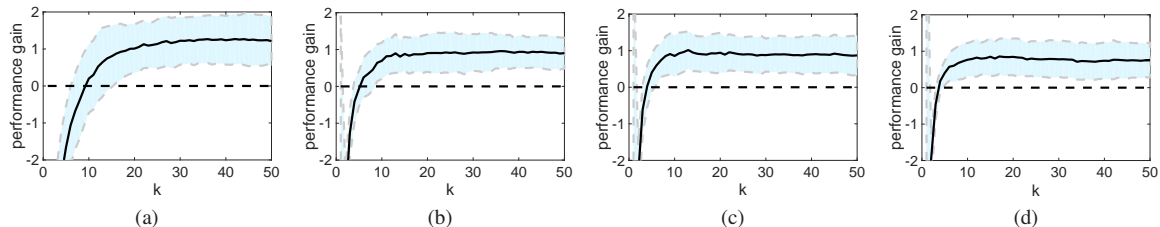


Fig. 12. Average performance gain of bi-DAKR as a function of k in multiple-to-multiple matching scenario. (a): rank-1. (b): rank-5. (c): rank-10. (d): rank-20.

TABLE VIII
COMPARISON ON COMPUTATION TIME COSTS.

Datasets	Size	Methods	Time
CHUK03	200	inv-DAKR	0.0356s
		bi-DAKR	0.0353s
		inv-DAKR+	0.0716s
		bi-DAKR+	0.0704s
		Zhong's[29]	0.2292s
PRID450s	450	inv-DAKR	0.0824s
		bi-DAKR	0.0804s
		inv-DAKR+	0.1683s
		bi-DAKR+	0.1648s
		Zhong's[29]	0.5682s
VIPeR	632	inv-DAKR	0.1563s
		bi-DAKR	0.1582s
		inv-DAKR+	0.2786s
		bi-DAKR+	0.2809s
		Zhong's[29]	0.8657s
GRID	1025	inv-DAKR	0.1302s
		bi-DAKR	0.1282s
		inv-DAKR+	0.3144s
		bi-DAKR+	0.3169s
		Zhong's[29]	1.2032s
Mars	12180	inv-DAKR	3.4126s
		bi-DAKR	3.7597s
		Zhong's[29]	33.4623s
Market-1501	19732	inv-DAKR	7.6503s
		bi-DAKR	8.6961s
		Zhong's[29]	88.3883s

V. CONCLUSION

We addressed the re-ranking problem for person ReID. Specifically, we have proposed two density-adaptive kernel based re-ranking approaches, named inv-DAKR and bi-DAKR, in which density-adaptive parameters are adopted to capture the local density information in gallery set. Moreover, we have extended inv-DAKR and bi-DAKR into the setting of re-ranking with the extra probe samples. Extensive experiments on six benchmark datasets have validated the efficiency and effectiveness of our proposals. Owing to the simplicity in implementation and lightweight computational cost, we hope that our proposals could be widely applied in real world person

ReID system.

ACKNOWLEDGMENT

R. Guo, J. Lin, and Y. Li are supported by the National Natural Science Foundation of China under Grant No. 61771066. C.-G. Li and J. Guo are supported by the National Natural Science Foundation of China under Grant No. 61876022.

REFERENCES

- [1] S. Gong, M. Cristani, S. Yan, and C. C. Loy, *Person Re-identification*. Springer, 2014.
- [2] N. Dalal and B. Triggs, "Histograms of oriented gradients for human detection," in *IEEE Conference on Computer Vision and Pattern Recognition*, 2005, pp. 886–893.
- [3] N. Dalal, B. Triggs, and C. Schmid, "Human detection using oriented histograms of flow and appearance," in *European Conference on Computer Vision*, 2006, pp. 428–441.
- [4] C. Liu, S. Gong, C. C. Loy, and X. Lin, "Person re-identification: what features are important?" in *European Conference on Computer Vision*, 2012, pp. 391–401.
- [5] Y. Yang, J. Yang, J. Yan, S. Liao, D. Yi, and S. Z. Li, "Salient color names for person re-identification," in *European Conference on Computer Vision*, vol. 8689, 2014, pp. 536–551.
- [6] J. Si, H. Zhang, C.-G. Li, and J. Guo, "Spatial pyramid-based statistical features for person re-identification: A comprehensive evaluation," *IEEE Transactions on Systems, Man and Cybernetics: Systems*, vol. 48, no. 7, pp. 1140–1154, 2018.
- [7] S. C. Dong, M. Cristani, M. Stoppa, L. Bazzani, and V. Murino, "Custom pictorial structures for re-identification," in *British Machine Vision Conference*, 2011, pp. 68.1–68.11.
- [8] N. Gheissari, T. B. Sebastian, and R. Hartley, "Person reidentification using spatiotemporal appearance," in *IEEE Conference on Computer Vision and Pattern Recognition*, 2006, pp. 1528–1535.
- [9] Y. Hu, S. Liao, Z. Lei, D. Yi, and S. Z. Li, "Exploring structural information and fusing multiple features for person re-identification," in *IEEE Conference on Computer Vision and Pattern Recognition*, 2013, pp. 794–799.
- [10] D. Gray and H. Tao, "Viewpoint invariant pedestrian recognition with an ensemble of localized features," in *European Conference on Computer Vision*, 2008, pp. 262–275.
- [11] X. Wang, G. Doretto, T. Sebastian, P. Tu, and J. Rittscher, "Shape and appearance context modeling," in *IEEE International Conference on Computer Vision*. Rio de Janeiro, 2007, pp. 1–8.

- [12] T. Matsukawa, T. Okabe, E. Suzuki, and Y. Sato, "Hierarchical gaussian descriptor for person re-identification," in *IEEE Conference on Computer Vision and Pattern Recognition*, 2016, pp. 1363–1372.
- [13] S. Liao, Y. Hu, X. Zhu, and S. Z. Li, "Person re-identification by local maximal occurrence representation and metric learning," in *IEEE Conference on Computer Vision and Pattern Recognition*, 2015, pp. 2197–2206.
- [14] J. Si, H. Zhang, C.-G. Li, J. Kuen, X. Kong, A. Kot, and G. Wang, "Dual attention matching networks for context-aware feature sequence based person re-identification," in *CVPR*, 2018.
- [15] J. Dai, Y. Zhang, H. Lu, and H. Wang, "Cross-view semantic projection learning for person re-identification," *Pattern Recognition*, vol. 75, pp. 63 – 76, 2018.
- [16] A. Franco and L. Oliveira, "Convolutional covariance features: Conception, integration and performance in person re-identification," *Pattern Recognition*, vol. 61, pp. 593–609, 2017.
- [17] J. V. Davis, B. Kulis, P. Jain, S. Sra, and I. S. Dhillon, "Information-theoretic metric learning," in *International Conference on Machine Learning*, 2007, pp. 209–216.
- [18] M. Dikmen, E. Akbas, T. S. Huang, and N. Ahuja, "Pedestrian recognition with a learned metric," in *Asian Conference on Computer Vision*, 2010, pp. 501–512.
- [19] M. Kostinger, M. Hirzer, P. Wohlhart, P. M. Roth, and H. Bischof, "Large scale metric learning from equivalence constraints," in *IEEE Conference on Computer Vision and Pattern Recognition*, 2012, pp. 2288–2295.
- [20] Z. Li, S. Y. Chang, F. Liang, T. S. Huang, L. L. Cao, and J. R. Smith, "Learning locally-adaptive decision functions for person verification," in *IEEE Conference on Computer Vision and Pattern Recognition*, 2013, pp. 3610–3617.
- [21] K. Q. Weinberger, J. Blitzer, and L. K. Saul, "Distance metric learning for large margin nearest neighbor classification," in *Conference on Neural Information Processing Systems*, 2006, pp. 1473–1480.
- [22] W. S. Zheng, S. Gong, and T. Xiang, "Person re-identification by probabilistic relative distance comparison," in *IEEE Conference on Computer Vision and Pattern Recognition*, 2011, pp. 649–656.
- [23] J. Si, H. Zhang, and C.-G. Li, "Regularization in metric learning for person re-identification," in *ICIP*, 2015, pp. 2309–2313.
- [24] L. Wu, Y. Wang, J. Gao, and X. Li, "Deep adaptive feature embedding with local sample distributions for person re-identification," *Pattern Recognition*, vol. 73, pp. 275–288, 2017.
- [25] J. Wang, S. Zhou, J. Wang, and Q. Hou, "Deep ranking model by large adaptive margin learning for person re-identification," *Pattern Recognition*, vol. 74, pp. 241 – 252, 2018.
- [26] Z. Zhao, B. Zhao, and F. Su, "Person re-identification via integrating patch-based metric learning and local salience learning," *Pattern Recognition*, vol. 75, pp. 90 – 98, 2018.
- [27] C. Liu, C. L. Chen, S. Gong, and G. Wang, "POP: Person re-identification post-rank optimisation," in *IEEE International Conference on Computer Vision*, 2013, pp. 441–448.
- [28] H. Wang, S. Gong, X. Zhu, and T. Xiang, "Human-in-the-loop person re-identification," in *European Conference on Computer Vision*, 2016, pp. 405–422.
- [29] Z. Zhong, L. Zheng, D. Cao, and S. Li, "Re-ranking person re-identification with k-reciprocal encoding," in *IEEE Conference on Computer Vision and Pattern Recognition*, 2017, pp. 3652–3661.
- [30] S. Bai, X. Bai, and Q. Tian, "Scalable person re-identification on supervised smoothed manifold," in *IEEE Conference on Computer Vision and Pattern Recognition*, 2017, pp. 3356–3365.
- [31] R. Yu, Z. Zhou, S. Bai, and X. Bai, "Divide and fuse: A re-ranking approach for person re-identification," in *British Machine Vision Conference*, 2017.
- [32] F. Korn and S. Muthukrishnan, "Influence sets based on reverse nearest neighbor queries," *Acm Sigmod Record*, vol. 29, pp. 201–212, 2000.
- [33] D. Qin, S. Gammeter, L. Bossard, T. Quack, and L. van Gool, "Hello neighbor: Accurate object retrieval with k-reciprocal nearest neighbors," in *IEEE Conference on Computer Vision and Pattern Recognition*, 2011, pp. 777–784.
- [34] Q. Leng, R. Hu, C. Liang, Y. Wang, and J. Chen, "Person re-identification with content and context re-ranking," *Multimedia Tools Appl.*, vol. 74, no. 17, pp. 6989–7014, 2015.
- [35] S. Bai and X. Bai, "Sparse contextual activation for efficient visual re-ranking," *IEEE Transactions on Image Processing*, vol. 25, no. 3, pp. 1056–1069, 2016.
- [36] Q. Leng, R. Hu, C. Liang, Y. Wang, and J. Chen, "Bidirectional ranking for person re-identification," in *IEEE International Conference on Multimedia and Expo*, 2013, pp. 1–6.
- [37] J. García, N. Martinel, A. Gardel, I. Bravo, G. L. Foresti, and C. Micheloni, "Discriminant context information analysis for post-ranking person re-identification," *IEEE Transactions on Image Processing*, vol. 26, no. 4, pp. 1650–1665, 2017.
- [38] R. Guo, C.-G. Li, Y. Li, and J. Lin, "Density-adaptive kernel ranking for person re-identification," in *Proceedings of International Conference on Pattern Recognition*, 2018, pp. 982–987.
- [39] L. Zelnik-manor and P. Perona, "Self-tuning spectral clustering," *Advances in Neural Information Processing Systems*, vol. 17, pp. 1601–1608, 2004.
- [40] C. L. Chen, T. Xiang, and S. Gong, "Time-delayed correlation analysis for multi-camera activity understanding," *International Journal of Computer Vision*, vol. 90, no. 1, pp. 106–129, 2010.
- [41] P. M. Roth, M. Hirzer, M. Köstinger, C. Belezni, and H. Bischof, "Mahalanobis distance learning for person re-identification," in *IEEE Conference on Computer Vision and Pattern Recognition*, 2014, pp. 247–267.
- [42] W. Li, R. Zhao, T. Xiao, and X. Wang, "DeepReID: Deep filter pairing neural network for person re-identification," in *IEEE Conference on Computer Vision and Pattern Recognition*, 2014, pp. 152–159.
- [43] L. Zheng, L. Shen, L. Tian, S. Wang, J. Wang, and Q. Tian, "Scalable person re-identification: A benchmark," in *IEEE International Conference on Computer Vision*, 2015, pp. 1116–1124.
- [44] L. Zheng, Z. Bie, Y. Sun, J. Wang, C. Su, S. Wang, and Q. Tian, "MARS: A video benchmark for large-scale person re-identification," in *European Conference on Computer Vision*, 2016, pp. 868–884.